Rabiee et al. International Journal of Mechanical and Materials Engineering (2021) 16:11
https://doi.org/10.1186/s40712-021-00133-7

International Journal of Mechanical and Materials Engineering

ORIGINAL PAPER Open Access

# Numerical model development to predict the behaviour of infant/neonate crash dummy restrained inside of an incubator under deceleration

A. Rabiee[1], H. Ghasemnejad[1*], N. Hitchins[2], J. Watson[3], J. Roberts[2] and M. Khoory[2]

## Abstract

In this paper, advanced finite element (FE) methods are developed to investigate the effect of deceleration on the crash dummy test complied with British Standard Engineering (BS EN 1789). These techniques, which are related to material modelling, joints and contacts, offer an advanced numerical model representing an infant incubator with all complex boundary conditions and design contents. It is shown that the response of an infant incubator is a function of the ratchet straps, the tension on the belts, the belt type and the distance of the belts from the edges of the incubator, which can significantly affect the experienced acceleration, by the infant. The validation process is performed against experimental studies and various case parameters such as crash dummy mass and negative acceleration impulse are discussed in detail. The developed numerical model is capable to predict the behaviour of the crash dummy and the incubator in terms of acceleration, trajectory and kinematics by less than 8% error.

**Keywords:** Incubator, Crash dummy, Biomechanics, LS-DYNA

## Introduction

An incubator is a piece of medical equipment suitable for a neonate or an infant to maintain environmental conditions, such as regulating temperatures, filter the breathing air and keeping babies warm. In recent years, the neonatal services have been developed based on response to local needs. According to the need of most of district general hospitals in neonatal care, it is required to establish a general quality standard protocol for neonatal intensive care. The major concept of neonatal, paediatric and reorganisation of midwifery, in general, was firstly published in 1999 entitled "Making a Difference". Two years later, in 2001, the Government's strategic plan was amended to include the changes required for neonatal care (D'Apolito 1991; Department of Health 1999; Department of Health 2001).

Inter-hospital transfer of babies has been an important part of neonatal care, however, individual hospitals were in charge of how this can be arranged and who would undertake it. This was amended when the concept of managed clinical networks (Department of Health 2003a, 2003b) was identified based on its importance as the rest of the care, and numbers of potential injuries that it can have on newborn babies or infants due to harsh braking or sudden acceleration. Neonates and infants can vary in weight, physiological condition, maturity states and other physiological complications that cause variation are body responses and tolerances in high forces (Department of Health 2003a; Department of Health 2003b; Department of Health 2004a; Department of Health 2004b; Medical Devices Agency n.d.; Mir 1997).

To maximise survivability in patients and member of staff subjected to inter-hospital transfer in ambulances,

* Correspondence: Hessam.Ghasemnejad@cranfield.ac.uk
[1]Department of Aerospace Engineering, Centre for Structures, Assembly and Intelligent Automation, Cranfield University, Cranfield, Wharley End, Bedford MK43 0AL, UK
Full list of author information is available at the end of the article

BS EN 1789:2007 (CEN 1789) was established. BS EN 1789 specifies requirements for ambulances intended to carry transport incubator systems along with requirements for the design, testing, performance and equipping of road ambulances used for the transport, monitoring, treatment and care of patients. This standard requires a dynamic testing of the fixations of the medical devices in the patient's compartment (between 8 and 12 g). To fixate an incubator to the stretcher inside of the patient's compartment, ratchet straps are used, while the stretcher can be fixed to its locking devices. The test assembly should be either accelerated or decelerated in the longitudinal, transverse and vertical directions with impact velocity of between 30 and 32 km/h in accordance to the deceleration impulse (Fig. 1a) (BS EN 1789:2007+A2:2014 2007).

Li et al. (Li et al. 2021) developed the key information of benchmark vehicles and high-strength steel front rails, which were designed to improve the crash performance of vehicle and reduce its structural mass (SM). In their work, the finite element analysis (FEA) of the front rail was carried out, and several dynamic drop testing were performed to verify the accuracy of finite element model. Emre İsa Albak (Albak 2021) studied multi-cell, multi-corner and adding edge-junction structures which are widely used approaches to enhance the crash characteristic of the thin-walled structures. In their work, the crashworthiness of twenty-one structures combining these three structures was examined under axial and oblique loading angles. The finite element models under axial loading were validated by experimental data from the literature and theoretical approach. Singh et al. (Singh et al. 2021) analysed the crashworthiness characteristics of the thin-walled tube, by introducing the combination of groove shape. A triple combination of groove shapes, V-shaped Rectangular, Circular Rectangular and Circular V shaped, has been taken for the analysis. These combined groove shapes were introduced at the tube

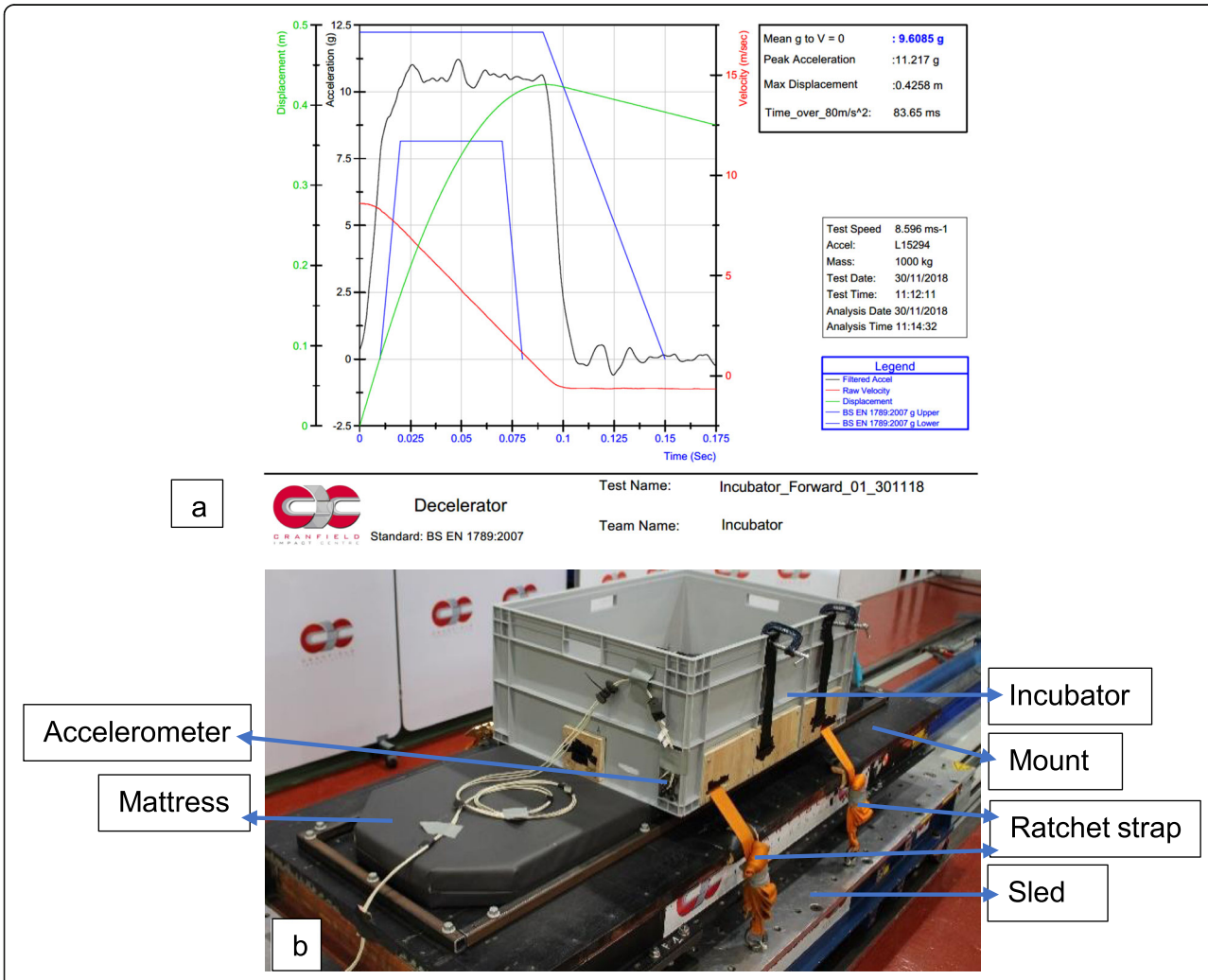


**Fig. 1** **a** A 10-g pulse, velocity and displacement read by the sled with BS EN 1789 guidelines and **b** experimental setup

outer wall. Four-, 6- and 8-groove specimens for each combined shape were prepared, and the effect of the variation of the number of grooves was also analysed. ABAQUS software was used for the numerical analysis of the groove tube and finds the crashworthiness characteristics such as peak load and energy absorption. Arjomandi Rad and Khalkhali (Arjomandi Rad and Khalkhali 2018) investigated the behaviour of such components under three-dimensional (3D) oblique loads in deterministic and probabilistic loading conditions. In this work, square tubes are tested experimentally, and results are utilized to validate numerical models. The primary outcome of this research is the effect of incidence angles on the energy-absorbing characteristics, as well as some remarkable trade-off design points obtained from various multiple-criteria decision-making (MCDM) methods. It was discovered that the obtained design points of the probabilistic study, which satisfied the reliability constraint, were roughly 60% more robust than the deterministic points.

Ofochebe et al. (Ofochebe et al. 2016) studied a new design protocol that attempts to overcome such problems in the evaluation of vehicle structure for crashworthiness. The implementation of the AEMS involved studying crash performance of vehicle components at various absorbable energy ratios based on a 2DOF lumped-mass-spring (LMS) vehicle impact model. This was used for the prompt prediction of useful parameter values in a given design problem. Wang et al. (Wang et al. 2010) proposed a time-based metamodeling technique for the vehicle design. The characteristics of the proposed method were the construction of a time-based objective function and establishment of a metamodel by support vector regression (SVR). They concluded that compared with other popular metamodel-based optimization methods, the design space of the proposed method was expanded to time domain. Thus, more information and features can be extracted in the expanded time domain. Ghadianlou and Bin Abdullah (Ghadianlou and Bin Abdullah 2013) studied the applied permanent damages of vehicle frontal door caused by pole impacts. In the side impact, the side door beam is responsible to absorb the most possible kinetic energy. Two significant parameters including material and geometry of a side door beam were discussed to reduce permanent damage of the door. Kathiresan (Kathiresan 2020) investigated the influences of different shapes, sizes and numbers of lateral cutouts at various locations on the load-bearing capacity; buckling behaviour and energy absorption characteristics of aluminium conical frusta under quasi-static axial loading condition from both experimental and numerical procedures. Baroutaji et al. (Baroutaji et al. 2017) analysed a broad survey of the literature, a comprehensive overview of the recent developments in the area of crashworthiness performance of TW tubes with a special focus on the topics that emerged in the last 10 years such as crashworthiness optimisation design and energy-absorbing responses of unconventional TW components including multicells tubes and functionally graded thickness tubes. Kecman (Kecman 1997) summarised the main points of the long-term engineering experience at Cranfield Impact Centre Ltd in the field of crashworthiness of thin-walled beams and joints in vehicle structures. The following subjects were covered: the 'hybrid' approach to crashworthiness design/analysis (where beams and joints are treated separately from complete structures), the deep-bending collapse of beams and joints from the points of view of static and dynamic testing and analytical prediction (models of hinge mechanisms, regression analysis, finite element analysis and from experimental databases).

In this paper, advanced finite element (FE) methods are developed to investigate the effect of deceleration on the crash dummy test complied with British Standard Engineering (BS EN 1789). These techniques, which are related to material modelling, joints and contacts, offer an advanced numerical model representing an infant incubator with all-complex boundary conditions and design contents. It is shown that the response of an infant incubator is a function of the ratchet straps, the tension on the belts, the belt type and the distance of the belts from the edges of the incubator, which can significantly affect the experienced acceleration by the infant.

In this paper, an 8-kg crash dummy between Q0 (a 6-week infant) and Q1 (a 12-month infant) (Q = dummy size) equivalent is designed. This enabled us to reduce the mass of the crash dummy and carry out further experiments as we did in this paper. A numerical model was developed based on this in-house crash dummy. A child differs from an adult not only in size but also in body segment proportions and anatomy. This dissimilarity in body segment proportions leads to a higher centre of gravity in a child, which affects the body kinematics in the event of an accident. This decreases the tolerance of a child to withstand high forces. The joint stiffness and bone density of a child differ from adults. Neonates and infants with heavy heads and weak neck musculature and young children are at a higher risk of cervical spine injuries in a frontal impact collision. Hence, to predict the behaviour of an infant/neonate subjected to a 10-g pulse, it was necessary to replicate the experimental data.

In the comparison of the experimental and numerical results, the maximum allowable margin of percentage error is 10%, as reviewed in (BS EN 1789:2007+A2:2014 2007; Li et al. 2021; Albak 2021; Singh et al. 2021; Arjomandi Rad and Khalkhali 2018; Ofochebe et al. 2016; Wang et al. 2010; Ghadianlou and Bin Abdullah

2013; Kathiresan 2020; Baroutaji et al. 2017; Kecman 1997). In general and according to the literature and British Standards, differences below 10% are referred to good and below 20% as acceptable (BS EN 1317-1:2010 n.d.; BS EN 1371-2:2010 n.d.; BS EN 4138:2012 n.d.; PD ISO/TR 21934-1 n.d.; BS EN 19364:2016 n.d.; BS EN 7862:2004 n.d.; Zhu and Huang 2018). The selected validation method for this study is the Roadside Safety Verification and Validation Program (RSVVP). This method is used in literature to compare experimental data with numerical outputs, and most importantly to validate the obtained curves using statistical methods tailored for crash analysis using ANOVA metrics and magnitude phases (Ray and Mongiardini 2009). The objective of the study in this paper is to study the behaviour of neonates experimentally and numerically under negative acceleration loading to provide better protection. The developed finite element model techniques and design variable studies of mass, velocity and accelerations will have significant implications more broadly for biomechanics and other related research areas.

## Materials and methods

### Experimental studies

The experimental studies were conducted at Cranfield Impact Centre (CIC), Cranfield University, UK. The Decelerator facility is connected to any components or dummies to predetermined deceleration (negative acceleration) pulses. According to BS EN 1789:2007, the required negative acceleration impulse is set at 10 g (see Fig. 1). The standard provides a graph (see Fig. 1a); two profiles are given at 8 g and 12 g; the test curve should be between the two; otherwise, the test is not valid (e.g. if the test curve crosses the 8-g or 12-g curve at any given time, the test should be repeated).

Sled testing is used to reproduce a desired dynamic condition in a controlled environment at a fraction of the cost of a real-case collision scenario or a full-scale crash test. The experimental setup has a sled, mount, mattress and a frame for the mattress, incubator, and two ratchet straps to restrain the incubator in the lateral direction of the sled. The mass of the crash dummy inside of the incubator is 8 kg. The sheet underneath of the dummy is attached to the incubator side walls with a five-point restraining system. The total mass of the setup is 1000 kg (see Fig. 1b). The ratchet strap hooks on to the sled, which is applied through the incubator by the provided slots and tightened belts. The belt should be tight enough so the width of the belt can bend up to a 90° angle. Two accelerometers are calibrated; one is mounted onto the incubator, and the other is mounted on the chest of the dummy. The box (incubator) weighs 6 kg, and an additional mass of 12 kg is added to the base to replicate the total mass of the designed incubator to 18 kg. The acceleration impulse, which is applied to the sled is extracted and used for the numerical model to improve the similarity. The displacement vs time and velocity vs time curves can also be compared with the results from numerical (FEM) analysis.

Tensile testing based on EN ISO 1492 was carried out on two types of belts, which are used for the five-point restraining system; the belts attach the sheet to the incubator. The size of each specimen was 15 cm in length with 10 mm/min test speed. The incubator was tested based on ASTM D638–14. The length of the specimen was 115 mm with 3-mm thickness with 10 mm/min test speed. The force–displacement curves obtained from experimental studies were compared with numerical results to calibrate the predictions. The belts are tested without pretension, and the thin webbing belt refers to the five-point restraining system, which is used for a dummy attached to the sheet, and wide webbing belt refers to the belt to restrain the sheet to the incubator. The calibration process is referring to the loading and unloading curves to match numerical results to experimental results. Experimental and finite element results are illustrated in Fig. 2. Four to six samples were tested per case under tensile test (pull test). To improve the prediction and accuracy of the model, tensile testing of the belts, sheet, and the incubator is calibrated in the model. Hence, in Fig. 2, the force–displacement curves indicate similar trends in all parts. This leads to a significant improvement in behavioural prediction. Once the belt is under tension, the model is implemented with the relative stress–strain curve, which leads to an accurate prediction of results.

### Finite element studies

In this section, a description of the numerical setup is outlined. The model consists of five components: sled, mattress, two belts and the incubator. The mass of the incubator is divided into eight sections; the incubator structure weighs 6 kg, and 12 kg is added to the base nodes to replicate the experimental setup, using Element_Mass_Node_Set. The mattress is modelled using Mat_Low_Density_Foam (Mat_057), and the incubator, sheet and sled are modelled using Mat_Piecewise (Mat_024); the safety belts and ratchet straps are modelled using Mat_Seatbelt_2D. Initial velocity is set to all nodes in the model and load–deflection curve for the foam (mattress) is implemented in the model. A mass of 20 kg was placed on the mattress, and the deflection was obtained experimentally. This was recreated in the model, and a mesh sensitivity was carried out accordingly. The final model is shown in Fig. 3.

A seven-joint dummy is designed in CAD software (SolidWorks), and the joints are modelled in Ls-PrePost. The geometry is modelled based on the experimental

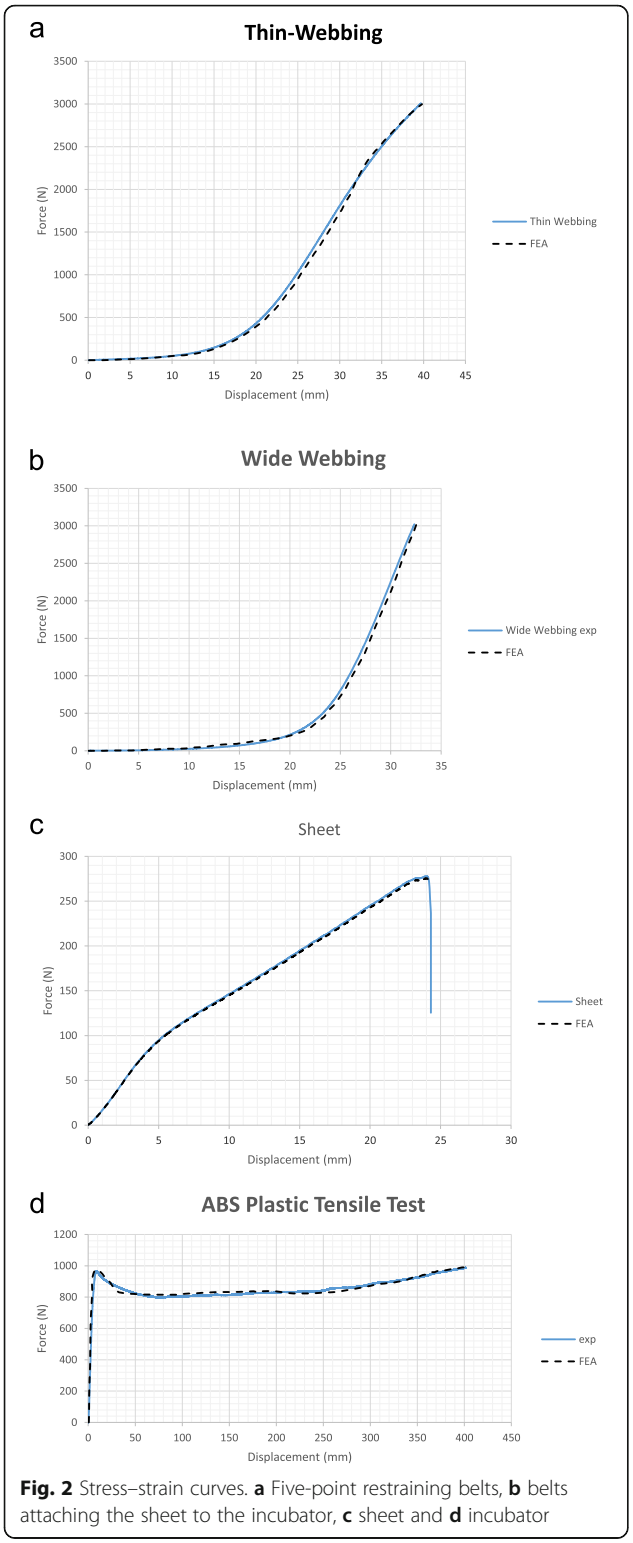


**Fig. 2** Stress–strain curves. **a** Five-point restraining belts, **b** belts attaching the sheet to the incubator, **c** sheet and **d** incubator

studies set up. The material formulation, size, mass and material card are shown in Table 1. In LS-DYNA, Mat_ 24, which is referred to as PIECEWISE, has 8 linear segments, which can be defined to reproduce an approximate non-linear stress–strain curve. This material card can also be used to input stress–strain curves from a tensile test as shown in Table 2. Mat_ B01 which is Seatbelt 2D is used to model the loading and unloading of the belts. Young's modulus is determined by LS-DYNA according to the loading curve, LLCID (Load curve identification for loading). The loading and unloading curves are represented by effective stress versus effective plastic strain for Mat_24 and strain/force with engineering strain for Mat_B01.

This FE model contains 61,471 nodes, 1252 seat belt elements, 37,512 shell elements, 18,756 solid elements (total 57,520 elements), and 17 parts or components and 8 inertia parts (for the dummy). Structural components and specific element types, which are used in the model, include fully integrated S/R solid (solid elements), Belytschko-Tsay (shell elements) and fully integrated Belytschko-Tsay membrane (shell elements).

In FEM, The function of the boundary conditions is to define and create constraints and loads. To simulate a crash scenario, the boundary conditions and all the acting loads that occur in the actual event need to be modelled, including gravitational loads (representing gravity force), coefficient of friction between the incubator and the mattress, belts and mattress, belts and incubator, dummy and safety belts, and finally dummy and mattress. The deceleration is modelled using Boundary_Prescribed_motion_set in the axial direction; this enables adding acceleration or deceleration to a set of predefined nodes. This recreates the sled condition, similar to the experiment, the sled undergoes a 10-g deceleration and the other components experience different g-forces due to the mass, restraining system, etc. Another method is Load_Body that creates a boundary in the model so all components experience the same force–deceleration rate, which is not suitable in this case. An initial velocity of 8.6 m/s was applied to all the nodes in the model to replicate the 31 km/h speed before the deceleration. Dynamic relaxation was enabled to determine the prestress caused by gravitational acceleration, which was modelled using Load_Body. The explicit dynamic relaxation in the transient analysis is used to preload the model including gravity, belt tension and mattress.

The joint of the crash dummy is modelled using Contrained_joint_spherical, which creates a 6-axis joint based on two opposite nodes of a given joint. If the nodes are misaligned, then torque is generated, and the part will rotate on the given axis. The joint stiffness degree of freedom is controlled and modelled between the two parts for the same joint, using Contrained_Joint) stiffness_Generalised. This card is defined using the part ID followed by a local coordinate system that is based on this local coordinate system (datum); the stop angle in degrees for negative or positive of x, y, and z rotations is defined based on elastic stiffness per unit radian for

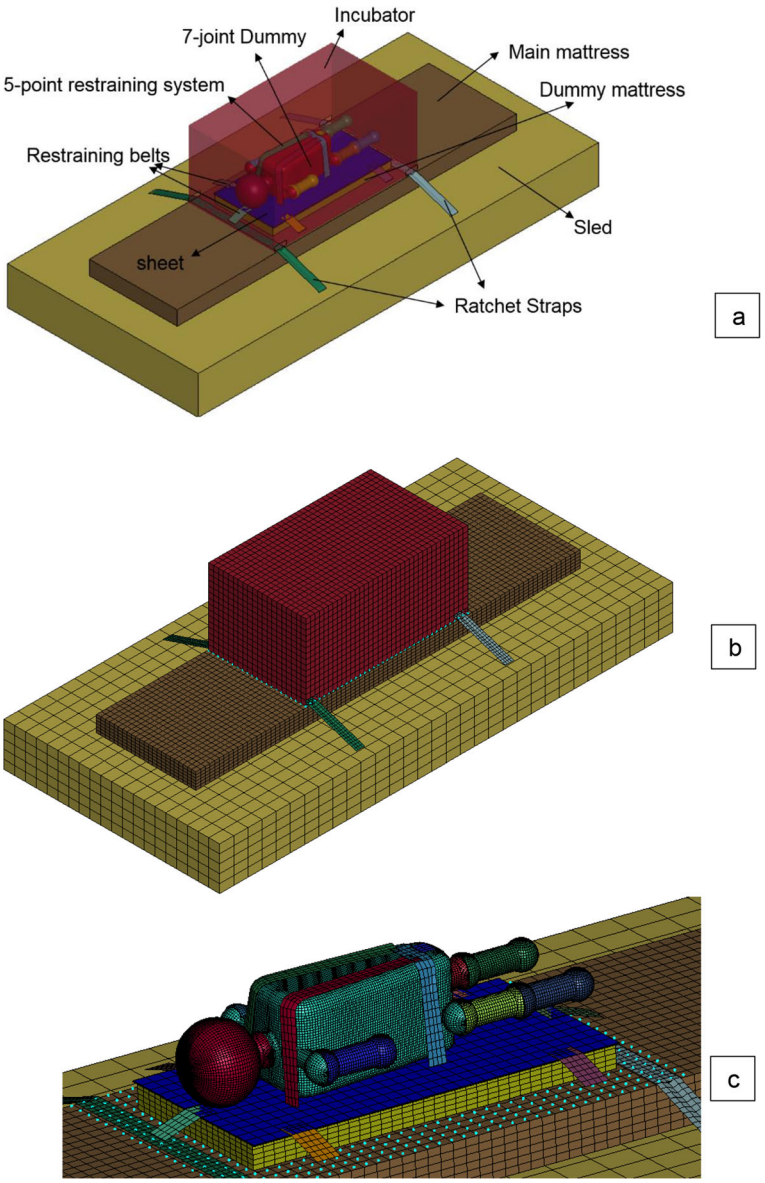


**Fig. 3 a** Final developed numerical model with all components, **b** mesh generation, **c** mesh and restraining system of the FEM crash dummy

**Table 1** Geometry, mass, element formulation and material card in LS-DYNA

| Component | Size: length, width, height (m) | Mass (kg) | Element formulation | Material card |
|---|---|---|---|---|
| Incubator | 0.75 × 0.45 × 0.35 | 18 | Belytschko-Tsay | Mat 24 |
| Main Mattress | 1.78 × 0.46 × 0.075 | 2.7 | Fully integrated S/R solid (solid elements) | Mat 57 |
| Sled | 2.1 × 1× 0.277 | 2.2.1.1.1. 968.8 | Fully integrated S/R solid (solid elements) | Mat 24 |
| Belt (×2) | 0.9 × 0.05 × 0.0012 | 1.5 | Fully integrated Belytschko-Tsay membrane | Mat B01 |
| Sheet | 0.625 × 0.315 × 0.002 | 0.25 | Fully integrated S/R solid (solid elements) | Mat 24 |
| Dummy mattress | 0.62 × 0.3 × 0.04 | 0.45 | Fully integrated S/R solid (solid elements) | Mat 57 |
| Belts (6) | 0.09 × 0.045 | 0.105 | Fully integrated Belytschko-Tsay membrane | Mat B01 |
| 5-point belt (as a whole) | 0.32 × 0.165 × 0.16 | 0.195 | Fully integrated Belytschko-Tsay membrane | Mat B01 |
| Dummy | 0.62 × 0.22 × 0.17 | 8 | Belytschko-Tsay | Mat 20 |

**Table 2** Mechanical properties of all components in the FE model

| Component | Material card | Young's modulus (EA) (GPa) | Poisson's ratio | Yield stress | Loading curve used | Unloading curve used | Mass per metre (kg) |
|---|---|---|---|---|---|---|---|
| Sled | 24 | 207 | 0.3 | 0.2 | Yes | | |
| Incubator | 24 | 1.029 | 0.3 | 0.15 | Yes | | |
| Mattress | 57 | 25 | | | | | |
| Belt (×2) (Ratchet strap) | B01 | 5.4 | 0.3 | | Yes | Yes | 0.07 |
| Sheet | 24 | 0.081 | 0.3 | 0.1 | Yes | | |
| Dummy mattress | 57 | 25 | | | | | |
| Belts (6) (sheet belts to incubator) | B01 | 0.54 | 0.3 | | Yes | Yes | 0.045 |

friction and stop angles for x, y and z rotations (see Table 3). The ESPH is elastic stiffness per unit radian for friction and stop angles for x rotation. The FMPH is frictional moment limiting value for x rotation. EST is elastic stiffness per unit radian for friction and stop angles for y rotation. FMT is frictional moment limiting value for y rotation. The ESPS is elastic stiffness per unit radian for friction and stop angles for z rotation. FMPS is frictional moment limiting value for z rotation. NSAP H is stop angle in degrees for negative x rotation. PSAP H is stop angle in degrees for positive x rotation. NSAT is stop angle in degrees for negative y rotation. PSAT is stop angle in degrees for positive y rotation. NSAPS is stop angle in degrees for negative z rotation, while PSAP S is stop angle in degrees for positive z rotation.

In this FE setup, 51 contact definitions were utilised as Contact_Tied_Surface_To_Surface to tie the mattress to the sled. Contact_Automatic_Surface_To_Surface was utilised between incubator (master) and the mattress (slave) with the static and dynamic coefficient of friction of 0.3 and 0.2, respectably (Zhu and Huang 2018). Two Contacts of Automatic_Surface_To_Surface were defined between mattress (slave) and belt 1 (master) and Belt 2 (master) with the static and dynamic coefficient of friction of 0.3 and 0.2 (Zhu and Huang 2018). Contact Tied_ Nodes_To_Surface was utilised to tie the Node_sets, which is created at the end of the belts to tie them to the sled. This contact definition was used to tie the incubator onto the belts, please see Table 4. To compare and evaluate the model performance, the sled outputs, which are displacement (m), velocity (m/s) and acceleration (g), were compared with the sled response in the numerical model.

## Results, discussions and validation

As neonates, infants and young children have weak neck musculature and heavy heads; this situation puts them at a higher risk of cervical spine injuries in a frontal impact collision. Hence, to predict the behaviour of an infant/ neonate subjected to 10-g pulse, it was necessary to perform the experimental studies. The safety belts stress–strain curves are crucial in these tests, as the crash dummy is a function of these belts. The purpose of the belt is to help absorb kinetic energy, and delay the energy transition to the incubator and to the infant to help reduce the initial high peak and instead have a steady increase of load. The ratchet straps, the belts restraining the sheet, which is attached to the main structure of the incubator, and the five-point restraining system that restrain the dummy are studied for the design of infant incubators.

The model-predicted results are validated against the experimentally obtained results, once both sets of data are extracted. The trend and the behaviour of both curves are studied known as curve observation, which also entails the time duration of the impulse and highest peak comparison. The most important factor is the area under the curves of force–time graphs (force or g-force multiplied by time), which is known as an impulse. Therefore, this

**Table 3** Constrained joint stiffness generalised input values

| Body part | ESPH | FMPH | EST | FMT | ESPS | FMPS | NSAPH | PSAPH | NSAT | PSAT | NSAPS | PSAPS |
|---|---|---|---|---|---|---|---|---|---|---|---|---|
| Right arm | 0.87 | 0.715 | 0.8 | 0.715 | 1.043 | 0.81 | − 116 | 3.54 | -3.5 | 4.2 | 168 | 5.4 |
| Upper right leg | 1.92 | 0.88 | 1.9 | 0.88 | 4.6 | 0.92 | − 32 | 2.2 | − 2.2 | 2.2 | − 16.5 | 16.5 |
| Left arm | 0.87 | 0.715 | 0.87 | 0.715 | 1.043 | 0.81 | − 3.54 | 116 | − 4.2 | 3.5 | − 5.4 | 168 |
| Upper left leg | 1.89 | 0.88 | 1.9 | 0.88 | 4.6 | 0.92 | − 2.2 | 32 | − 2.2 | 2.2 | − 16.5 | 16.5 |
| Head | 2.9 | 2.28 | 2.1 | 2 .27 | 3.3 | 1.89 | − 12.3 | 22.5 | − 30.3 | 30.3 | − 20.4 | 20.4 |
| Lower left leg | 1.44 | 0.12 | 1.5 | 0.1 | 6.7 | 2.8 | 0 | 60 | − 0.1 | 0.1 | − 0.1 | 0.1 |
| Lower right leg | 1.52 | 0.1 | 1.4 | 0.12 | 6.7 | 2.8 | 60 | 0 | − 0.1 | 0.1 | − 0.1 | 0.1 |

**Table 4** Contact definition

| Number | Contact | Components | Static coefficient of friction | Dynamic coefficient of friction |
|---|---|---|---|---|
| 1 | Contact_Tied_Surface_To_Surface | Incubator (master)<br>Mattress (slave) | | |
| 2 | Contact_Automatic_Surface_To_Surface | Incubator (slave)<br>Mattress (master) | 0.3 | 0.2 |
| 3 | Contact_Automatic_Surface_To_Surface | Mattress (slave)<br>Main belt 1 (master) | 0.3 | 0.2 |
| 4 | Contact_Automatic_Surface_To_Surface | Mattress (slave)<br>Main belt 2 (master) | 0.3 | 0.2 |
| 5 | Contact_Tied_Nodes_To_Surface | Belt 1 node set (slave)<br>Sled (master) | | |
| 6 | Contact_Tied_Nodes_To_Surface | Belt 2 node set (slave)<br>Sled (master) | | |
| 7 | Contact_Tied_Nodes_To_Surface | Belt 3 node set (slave)<br>Sled (master) | | |
| 8 | Contact_Tied_Nodes_To_Surface | Belt 4 node set (slave)<br>Sled (master) | | |
| 9 | Contact_Tied_Nodes_To_Surface | Incubator (slave)<br>Belt 1 (master) | | |
| 10 | Contact_Tied_Nodes_To_Surface | Incubator (slave)<br>Belt 2 (master) | | |
| 11 | Contact_Automatic_Surface_To_Surface | Torso (slave)<br>Incubator (master) | 0.45 | 0.25 |
| 12 | Contact_Automatic_Surface_To_Surface | Right arm (slave)<br>Incubator (master) | 0.45 | 0.25 |
| 13 | Contact_Automatic_Surface_To_Surface | Upper leg right (slave)<br>Incubator (master) | 0.45 | 0.25 |
| 14 | Contact_Automatic_Surface_To_Surface | Upper leg right (slave)<br>Incubator (master) | 0.45 | 0.25 |
| 15 | Contact_Automatic_Surface_To_Surface | Left arm (slave)<br>Incubator (master) | 0.45 | 0.25 |
| 16 | Contact_Automatic_Surface_To_Surface | Lower leg right (slave)<br>Incubator (master) | 0.45 | 0.25 |
| 17 | Contact_Automatic_Surface_To_Surface | Lower leg left (slave)<br>Incubator (master) | 0.45 | 0.25 |
| 18 | Contact_Automatic_Surface_To_Surface | Head (slave)<br>Incubator (master) | 0.45 | 0.25 |
| 19 | Contact_Automatic_Surface_To_Surface | Torso (slave)<br>Dummy mattress (master) | 0.45 | 0.25 |
| 20 | Contact_Automatic_Surface_To_Surface | Right arm (slave)<br>Dummy mattress (master) | 0.45 | 0.25 |
| 21 | Contact_Automatic_Surface_To_Surface | Upper leg right (slave)<br>Dummy mattress (master) | 0.45 | 0.25 |
| 22 | Contact_Automatic_Surface_To_Surface | Upper leg right (slave)<br>Dummy mattress (master) | 0.45 | 0.25 |
| 23 | Contact_Automatic_Surface_To_Surface | Left arm (slave)<br>Dummy mattress (master) | 0.45 | 0.25 |
| 24 | Contact_Automatic_Surface_To_Surface | Lower leg right (slave)<br>Dummy mattress (master) | 0.45 | 0.25 |
| 25 | Contact_Automatic_Surface_To_Surface | Lower leg left (slave)<br>Dummy mattress (master) | 0.45 | 0.25 |
| 26 | Contact_Automatic_Surface_To_Surface | Head (slave)<br>Dummy mattress (master) | 0.45 | 0.25 |

**Table 4** Contact definition *(Continued)*

| Number | Contact | Components | Static coefficient of friction | Dynamic coefficient of friction |
|---|---|---|---|---|
| 27 | Contact_Automatic_Surface_To_Surface | Sheet (slave)<br>Dummy mattress (master) | 0.3 | 0.2 |
| 28 | Contact_Automatic_Surface_To_Surface | Dummy belt 1 (slave)<br>Dummy (Torso) (master) | 0.88 | 0.88 |
| 29 | Contact_Automatic_Surface_To_Surface | Dummy belt 2 (slave)<br>Dummy (Torso) (master) | 0.88 | 0.88 |
| 30 | Contact_Automatic_Surface_To_Surface | Dummy belt 3 (slave)<br>Dummy (Torso) (master) | 0.88 | 0.88 |
| 31 | Contact_Automatic_Surface_To_Surface | Dummy belt 4 (slave)<br>Dummy (Torso) (master) | 0.88 | 0.88 |
| 32 | Contact_Tied_Surface_To_Surface | Incubator (Slave)<br>Dummy mattress (Master) | | |
| 33 | Contact_Tied_Nodes_To_Surface | Sheet belt 1 (Slave)<br>Sheet (master) | | |
| 34 | Contact_Tied_Nodes_To_Surface | Sheet belt 2 (Slave)<br>Sheet (master) | | |
| 35 | Contact_Tied_Nodes_To_Surface | Sheet belt 3 (Slave)<br>Sheet (master) | | |
| 36 | Contact_Tied_Nodes_To_Surface | Sheet belt 4 (Slave)<br>Sheet (master) | | |
| 37 | Contact_Tied_Nodes_To_Surface | Sheet belt 5 (Slave)<br>Sheet (slave) | | |
| 38 | Contact_Tied_Nodes_To_Surface | Sheet belt 6 (Slave)<br>Sheet (master) | | |
| 39 | Contact_Tied_Nodes_To_Surface | Sheet belt 1 (Slave)<br>Incubator (master) | | |
| 40 | Contact_Tied_Nodes_To_Surface | Sheet belt 2 (Slave)<br>Incubator (master) | | |
| 41 | Contact_Tied_Nodes_To_Surface | Sheet belt 3 (Slave)<br>Incubator (master) | | |
| 42 | Contact_Tied_Nodes_To_Surface | Sheet belt 4 (Slave)<br>Incubator (master) | | |
| 43 | Contact_Tied_Nodes_To_Surface | Sheet belt 5 (Slave)<br>Incubator (master) | | |
| 44 | Contact_Tied_Nodes_To_Surface | Sheet belt 6 (Slave)<br>Incubator (master) | | |
| 45 | Contact_Tied_Nodes_To_Surface | Dummy belt 1 (Slave)<br>sheet (master) | | |
| 46 | Contact_Tied_Nodes_To_Surface | Dummy belt 2 (Slave)<br>sheet (master) | | |
| 47 | Contact_Tied_Nodes_To_Surface | Dummy belt 3 (Slave)<br>sheet (master) | | |
| 48 | Contact_Tied_Nodes_To_Surface | Dummy belt 4 (Slave)<br>sheet (master) | | |
| 49 | Contact_Tied_Nodes_To_Surface | Dummy belt 2 (Slave)<br>Dummy belt 1 (master) | | |
| 50 | Contact_Tied_Nodes_To_Surface | Dummy belt 3 (Slave)<br>Dummy belt 1 (master) | | |
| 51 | Contact_Tied_Nodes_To_Surface | Dummy belt 3 (Slave)<br>Dummy belt 1 (master) | | |

technique enables designers to find the changes in the momentum by finding the area under a force–time graph. The FE results indicate close agreement between displacement, velocity and acceleration (see Fig. 4).

Numerical and experimental data is compared based on the area under the curves. This method is vastly used in the field of impact mechanics to compare and evaluate numerical results with experimental data. Figure 5 shows the impulse of the incubator with the dummy and the mean force of both experiment and numerical are 9 g and 8.2 g, respectively. In this case, the percentage error is 8.3%. Figure 6 shows the dummy impulse and the mean force for both experimental and numerical results, 10 g and 11 g respectively. In this case, the percentage error is 8%, which remained below the margin of 10%, and both are within the acceptable range. Various stages of FE kinematic subjected to 10 g are illustrated in Figs. 7 and 8.

The area under each curve is calculated, and the error percentage is obtained in respect to experimental data. In Excel, the formula used to obtain the area for each point is (B1 + B2)/2 × (A2 − A1) followed through the column until all points on the graphs are covered; the sum function is used to get the total area. Once the area under the curve of both data sets is obtained, the percentage error in respect to the experimental data is calculated using the following function on excel, (SUM FEA − SUM EXP) / SUM EXP × 100. This can also be written as the average force along with the time duration. This is the mean force of the impulse. The mean forces of both experiment and numerical are close, 9.16 g and 8.27 g respectively (round up by two significant figures). The percentage error is calculated to be 8.32%.

## Design variables

Changing the mass of the dummy and the negative acceleration impulse are chosen in this section because the these two are the main variables in different

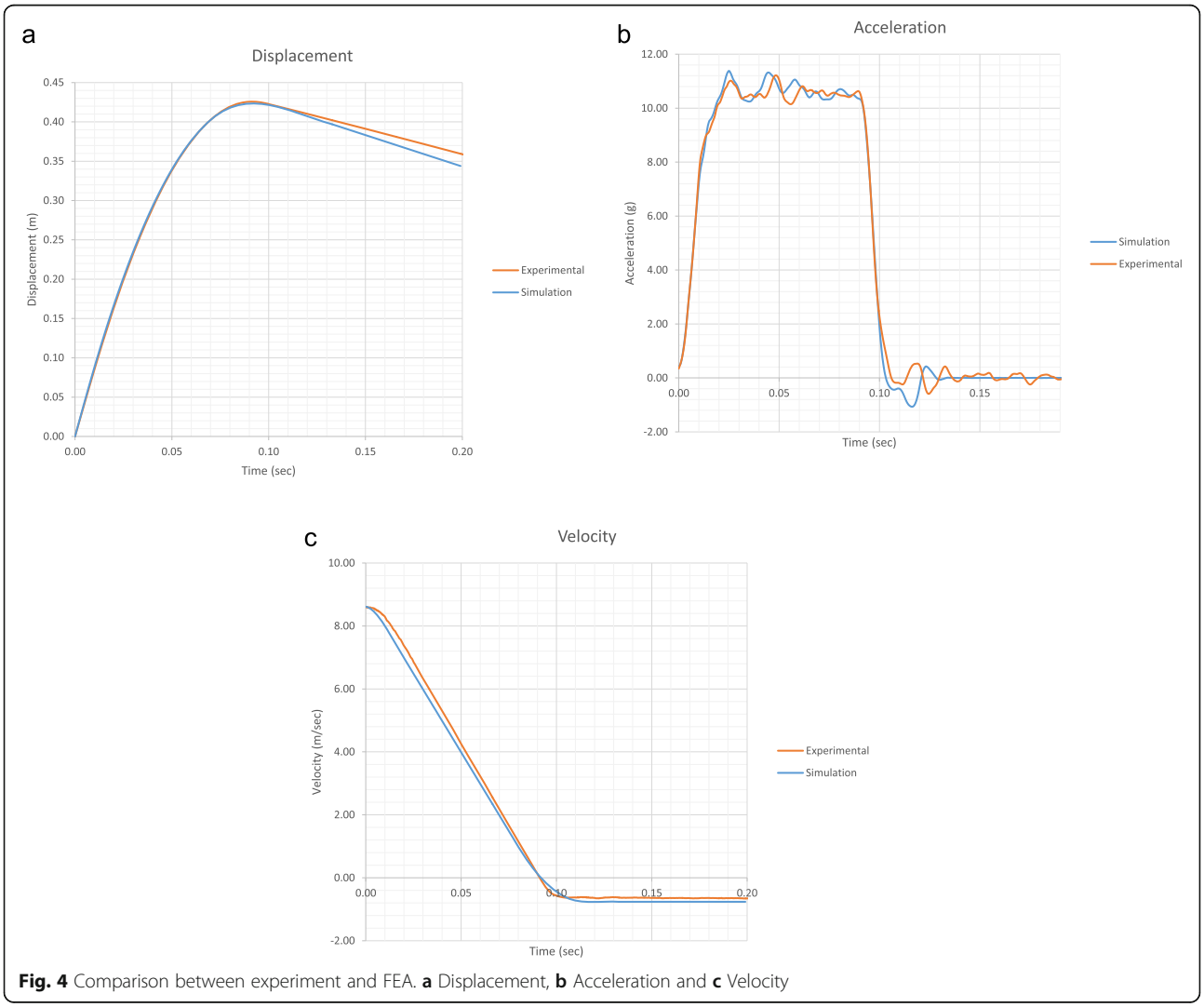


**Fig. 4** Comparison between experiment and FEA. **a** Displacement, **b** Acceleration and **c** Velocity

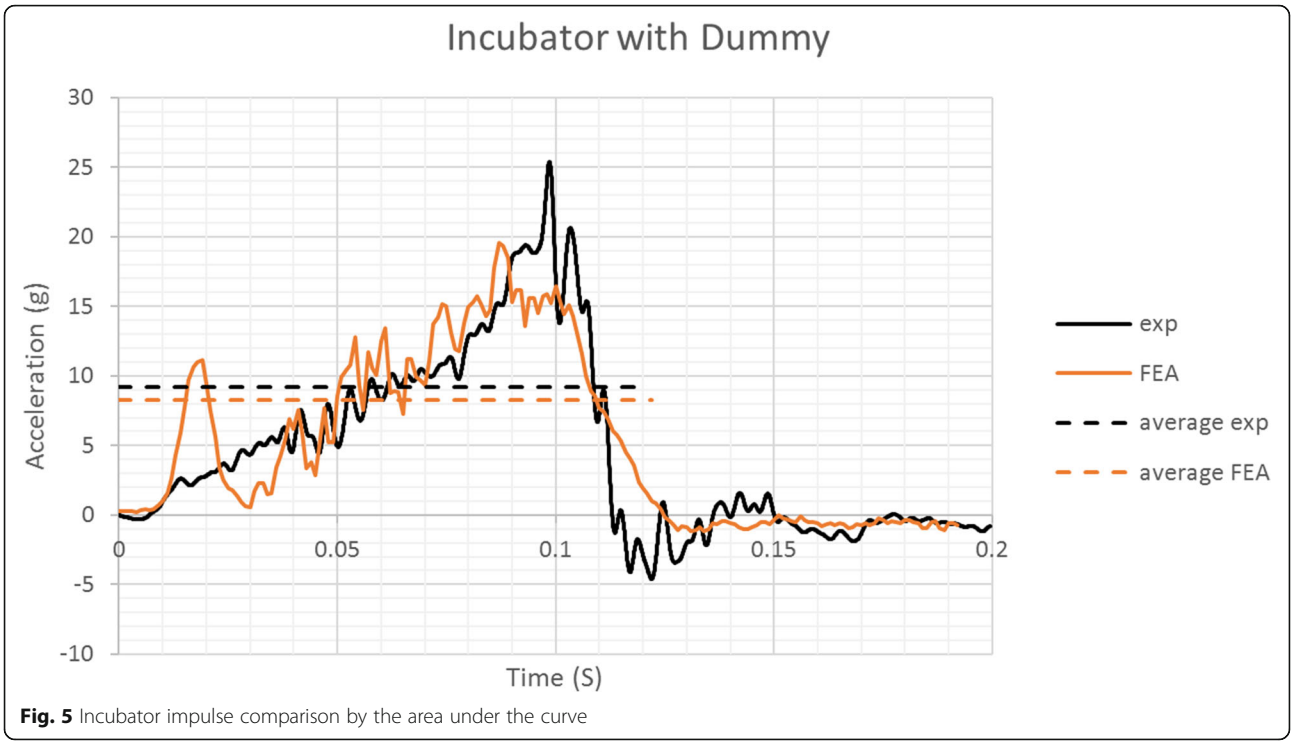


**Fig. 5** Incubator impulse comparison by the area under the curve

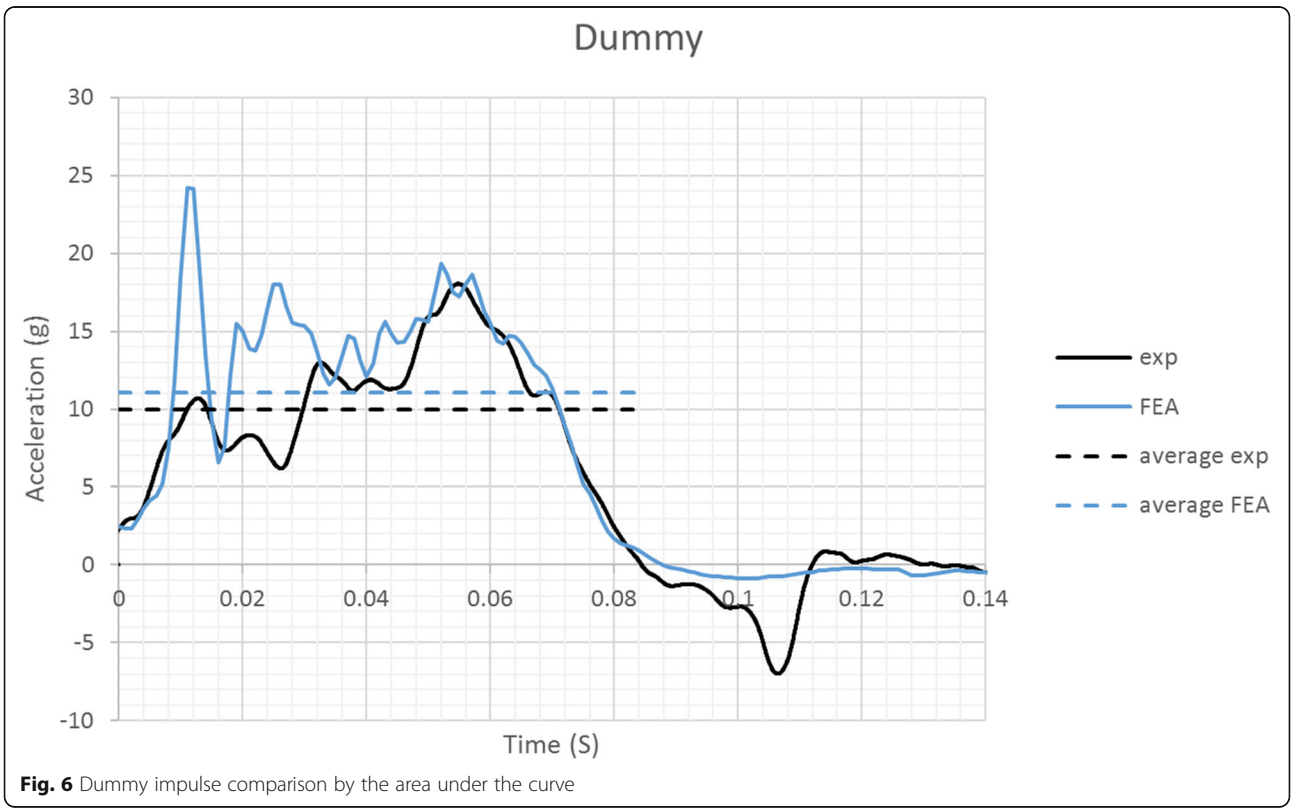


**Fig. 6** Dummy impulse comparison by the area under the curve

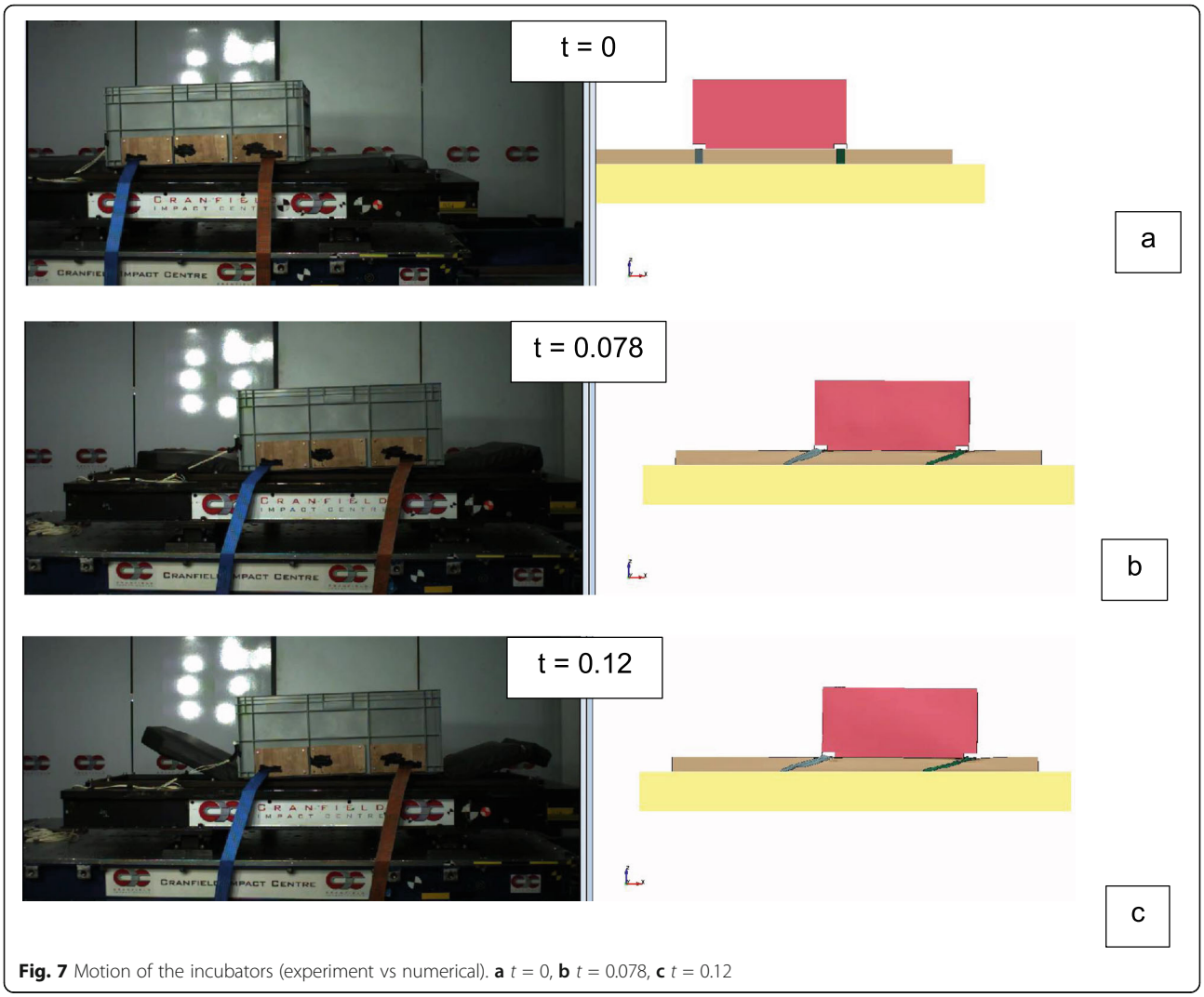


**Fig. 7** Motion of the incubators (experiment vs numerical). **a** $t = 0$, **b** $t = 0.078$, **c** $t = 0.12$

scenarios. For instance, the mass of a neonate or infant is subjected to variation, anything from 1 to 8 kg, and also, the negative acceleration is subjected to variation, for instance harsh braking.

### Dummy mass

In this model, the mass of the dummy is reduced to 6.3 kg, 4 kg and 2 kg from the original mass of 8 kg which was designed and validated in the Results, discussions and validation section. The simulation setup is unchanged from the validated model and the only parameter that was changed is the mass of the dummy. The two legends shown in Fig. 9 are very similar, and the differences are in the duration and initiation of the curve. In all cases, by reducing the mass of the dummy, the acceleration increases. This is because the force remains the same, and acceleration increases by reducing the mass.

### The 12-g and 8-g pulse

In this model, the mass of the dummy is kept as 8 kg. The simulation setup is unchanged from the validated model and variable parameter is the deceleration impulse. According to BS EN 1789:2007, 8-g and 12-g impulses are used to compare the acceleration rate of the dummy and the incubator. At 8-g impulse, the velocity is set to 30 km/h and at 12-g impulse, the velocity is set to 32 km/h as stated in the standard. The duration of the impulse and the maximum peak of the curve is more than 5 g compared with 10 g. In both graphs, the legend representing 10 g, is from the validated simulation. At 12-g impulse, the acceleration duration is increased and the peak reaches a spike of 38 g at 0.094 s, (see Fig. 10). In Fig. 11, the legends indicate the acceleration that the chest of the dummy experienced during the test. The duration and the maximum peak are significantly reduced at 8-g impulse. The maximum peak reaches 31-g under 12-g impulse.

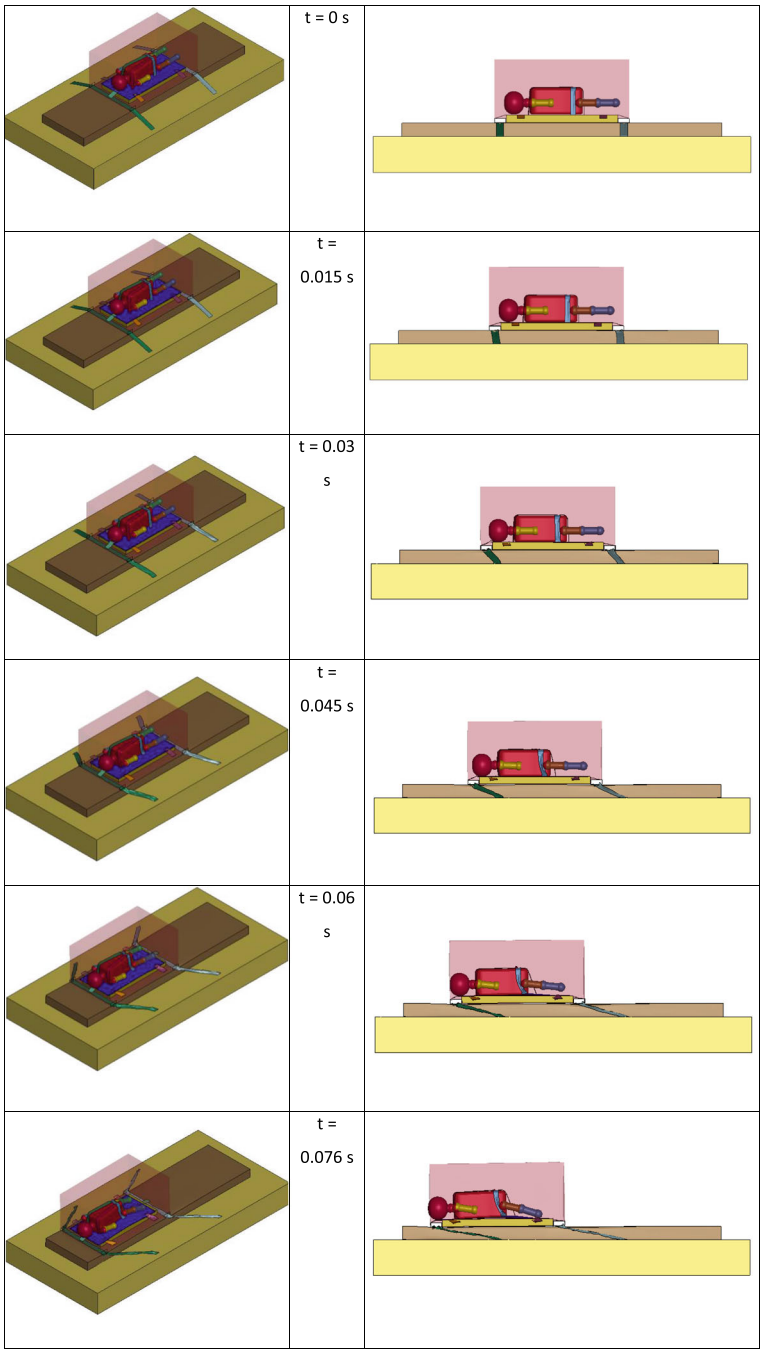


**Fig. 8** Various stages of kinematics subjected to 10 g

## Conclusions

The infant or neonate differs structurally from the adult in a number of ways which is critical to the design for protection against impact forces and for adequate occupant restraint systems; they have higher centre of gravity than child and adults, and this also depends on how premature the newborn or infant is. The body size proportions, muscle bone and ligamentrus strengths for instance are different and thus crash protection for occupant need special consideration. In CEN 1789 generally covers the fixation of the incubator and to avoid it being a projectile in case of a sudden acceleration or deceleration. Thus, in this paper, a robust finite element model is developed to predict the behaviour of an incubator including an 8-kg dummy under various impulses and crash dummy masses. The prediction of the finite

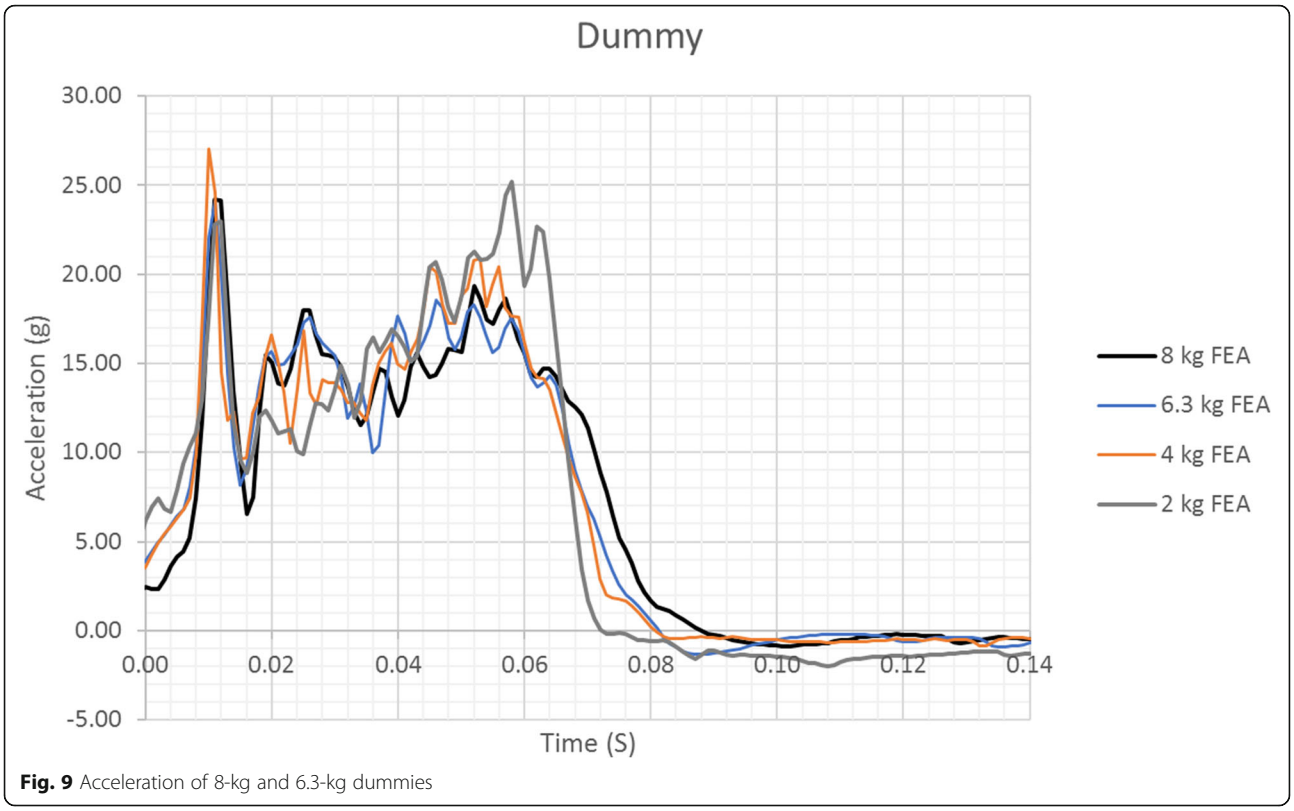


**Fig. 9** Acceleration of 8-kg and 6.3-kg dummies

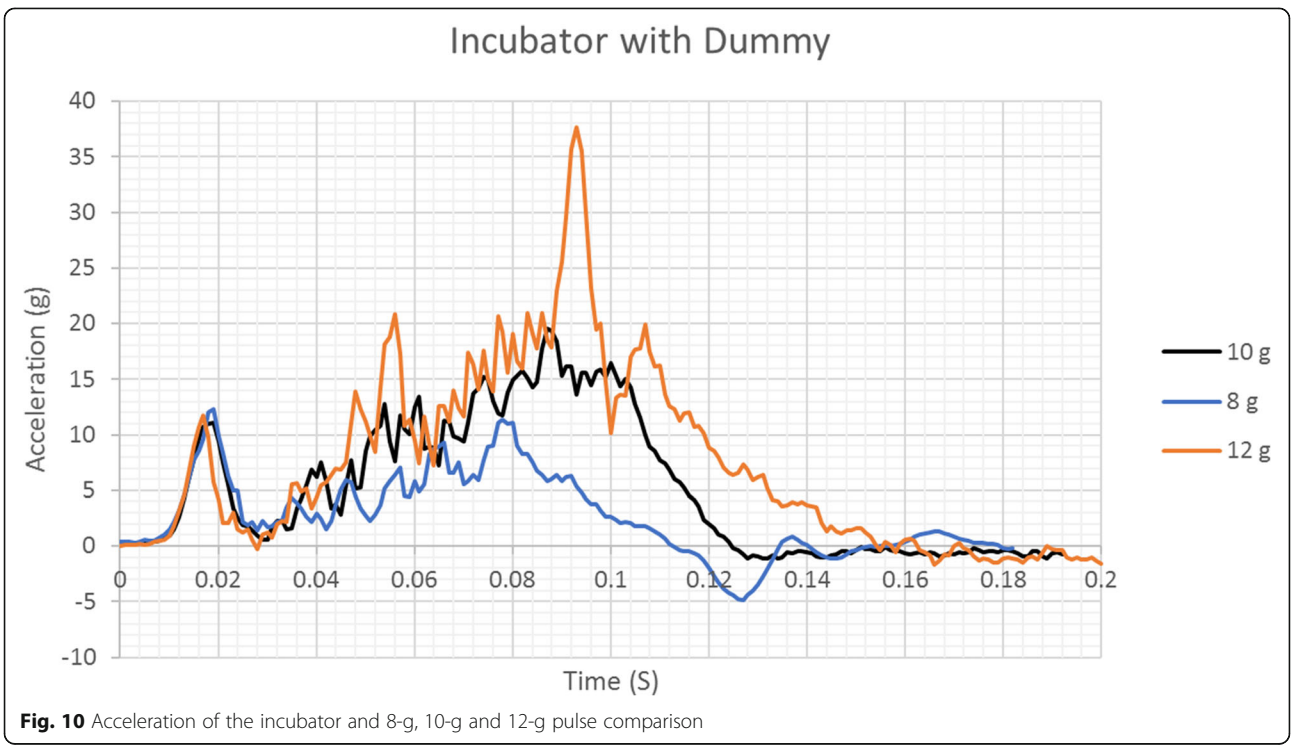


**Fig. 10** Acceleration of the incubator and 8-g, 10-g and 12-g pulse comparison

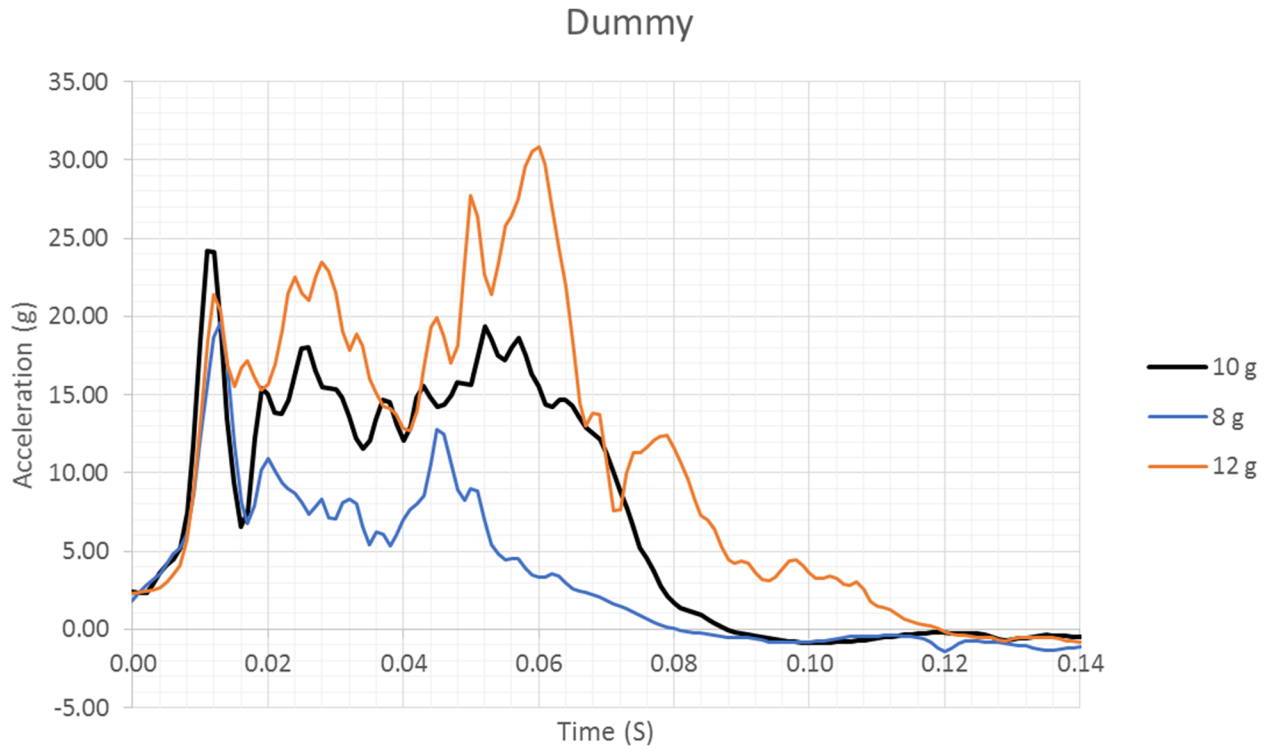


**Fig. 11** Acceleration of the dummy at 8 g, 10 g and 12 g

element model is 8% compared with experimental studies. This accuracy is due to the modelling technique applied to the safety belts. It was shown that an incubator is a function of the ratchet straps, the tension on the belts, the belt type and the distance of the belts from the edges of the incubator, which can significantly affect the experienced acceleration, by the infant. The distance of the ratchet straps from the edges of the incubator determine the stability of the incubator on the mattress, and it reduces the vibration due to the negative acceleration load. Therefore, the overall stability improves. Similarly, the dummy is a function of three belt setups, the ratchet straps, the belts restraining the sheet and the five-point restraining system. These factors change in every experiment and therefore influence the percentage error compared with the numerical studies. The robustness of our FE model is dependent on the stresses that belts encountered during the test. This threshold can be checked by the input stress–strain curves. Therefore, the prediction of the model is limited to the input data, if the range of the material stress–strain curves exceeds, the input then the model is no longer reliable.

By changing the mass of the dummy, the acceleration rate that the dummy experiences increases, as the force remains the same, and the mass is reduced, $F = m \times a$, and acceleration increases. The differences between 8 and 2 kg is severe, and it is necessary to account for the bone density and joint stiffness of a neonate that experiences higher force than a heavier infant; therefore, the survivability of a neonate with lower body mass is lower. The inside of the incubator should have enough room for the infant or neonate to avoid any contact with the walls in acceleration or deceleration.

In 12 g and 8 g, which are the upper and lower range limits of the BS EN 1789:2007 standard, the velocity is 32 km/h and 30 km/h respectively. To establish the importance of the deceleration rate on the incubator and the dummy, these scenarios were also studied. The worse-case scenario is a 2-kg neonate subjected to 12-g impulse.

The loading and unloading input curves are followed, and LS-DYNA calculates the Young's modulus. As long as the loading and unloading curves for the belts and incubator are not exceeded, changing other parameters wouldn't significantly deteriorate the results compared with relative experiment. The loading and unloading curves can be calculated and converted depending on the material model using Fig. 4 curves.

**Acknowledgements**
Not applicable

**Authors' contributions**
AR, HG, NH, JW, JR and MK read and corrected the manuscript. The authors read and approved the final manuscript.

**Funding**
InnovateUK is greatly acknowledged for funding this research.

**Availability of data and materials**
All data generated or analysed during this study are included in this published article.

## Declaration

**Competing interests**
The authors declare that they have no competing interests.

**Author details**
[1]Department of Aerospace Engineering, Centre for Structures, Assembly and Intelligent Automation, Cranfield University, Cranfield, Wharley End, Bedford MK43 0AL, UK. [2]mOm Incubators, EC1N 8LR, London, UK. [3]Cranfield Impact Centre, Cranfield University, Cranfield, Wharley End, Bedford MK43 0AL, UK.

Received: 22 December 2020 Accepted: 19 July 2021
Published online: 31 July 2021

**References**

Albak, E. İ. (2021). Crashworthiness design for multi-cell circumferentially corrugated thin-walled tubes with sub-sections under multiple loading conditions. *Thin Walled Struct*, *164*, 107886. https://doi.org/10.1016/j.tws.2021.107886.
Arjomandi Rad, M., & Khalkhali, A. (2018). Crashworthiness multi-objective optimization of the thin-walled tubes under probabilistic 3D oblique load. *Mater. Des.*, *156*, 538–557. https://doi.org/10.1016/j.matdes.2018.07.008.
A. Baroutaji, M. Sajjia, A. Olabi, Metallic thin-walled tubes for crashworthiness applications: a reference guide. Reference Module in Materials Science and Materials Engineering, 2017.
BS EN 1317-1:2010. (2010). Road restraint system – part 1: terminology and general criteria for test methods.
BS EN 1371-2:2010. (2010). Road restraint structures – part 2: performance classes, impact tests acceptance criteria and test methods for safety barriers including vehicle parapets.
BS EN 1789:2007+A2:2014 (2007). *Medical vehicles and their equipment. Road ambulances*. London: British Standards Institute.
BS EN 19364:2016. (2016). Passenger cars. Vehicle dynamic simulation and validation. Steady-state circular driving behaviour.
BS EN 4138:2012. (2012). Passenger cars. Steady-state circular driving behaviour. Open-loop test methods.
BS EN 7862:2004. (2004). Road vehicles. Sled test procedure for the evaluation of restraint systems by simulation of frontal collisions.
D'Apolito, K. (1991). What is an organized infant. *Neonatal Network*, *10*(1), 23–29.
Department of Health (1999). *Making a difference*. London: The Stationery Office.
Department of Health (2001). *Seeking consent: working with children*. London: DH.
Department of Health (2003a). *Neonatal intensive care services: paper of the department of health expert working group*. London: DH.
Department of Health (2003b). *Neonatal intensive care review: strategy for improvement*. London: DH.
Department of Health (2004a). *Changes for children – every child matters*. London: DH.
Department of Health (2004b). *National service framework for children, young people and maternity services*. London: DH.
Ghadianlou, A., & Bin Abdullah, S. (2013). Crashworthiness design of vehicle side door beams under low-speed pole side impacts. *Thin Walled Struct*, *67*, 25–33. https://doi.org/10.1016/j.tws.2013.02.004.
Kathiresan, M. (2020). Influence of shape, size and location of cutouts on crashworthiness performance of aluminium conical frusta under quasi-static axial compression. *Thin Walled Struct*, *154*, 106793. https://doi.org/10.1016/j.tws.2020.106793.
Kecman, D. (1997). An engineering approach to crashworthiness of thin-walled beams and joints in vehicle structures. *Thin Walled Struct*, *28*(3–4), 309–320. https://doi.org/10.1016/S0263-8231(97)00049-9.
Li, Q. Q., Li, E., Chen, T., Wu, L., Wang, G. Q., & He, Z. C. (2021). Improve the frontal crashworthiness of vehicle through the design of front rail. *Thin Walled Struct*, *162*, 107588. https://doi.org/10.1016/j.tws.2021.107588.
Medical Devices Agency. (1995). Transport of neonates in ambulances: guidance of the TINA Project UK, London: DH
Mir, N. (1997). *Manual of neonatal transfer*. Manchester: E Petch Printers.
Ofochebe, S. M., Enibe, S. O., & Ozoegwua, C. G. (2016). Absorbable energy monitoring scheme: new design protocol to test vehicle structural crashworthiness. *Heliyon.*, *2*(5).
PD ISO/TR 21934-1. (2021). Road vehicles - prospective safety performance assessment of pre-crash technology by virtual simulation. Part 1: state-of-the-art and general method overview
Ray, M., & Mongiardini, M. (2009). *Road Safety Verification and Validation Program (RSVVP) – user's manual*. Worcester Polytechnic Institute (WPI), Massachusetts, US.
Singh, S. K., Pandey, R., & Upadhyay, A. (2021). A numerical study on combined effects of groove shape and numbers on crashworthiness characteristics of thin-walled tube. *Mater Today*, *44*(6), 4381–4386.
Wang, H., Li, G. Y., & Li, E. (2010). Time-based metamodeling technique for vehicle crashworthiness optimization. *Comput Methods Appl Mechan Engineer*, *199*(37–40), 2497–2509. https://doi.org/10.1016/j.cma.2010.04.002.
Zhu, F., Huang, Y. FTSS FEA dummy models update: SID-IIs small side impact dummy model and others. 4th European LS-DYNA Users Conference 2018.

## Publisher's Note